Correlation-assisted quantized charge pumping

Jacob A. Marks, Michael Schüler, Jan C. Budich, and Thomas P. Devereaux

Phys. Rev. B **103**, 035112 — Published 11 January 2021

DOI: 10.1103/PhysRevB.103.035112

Correlation-Assisted Quantized Charge Pumping

Jacob A. Marks,[1,2,*] Michael Schüler,[2,†] Jan C. Budich,[3] and Thomas P. Devereaux[4,2]

[1]*Physics Department, Stanford University, Stanford, CA 94035, USA*
[2]*Stanford Institute for Materials and Energy Sciences (SIMES), SLAC National Accelerator Laboratory, Menlo Park, CA 94025, USA*
[3]*Institute of Theoretical Physics, Technische Universität Dresden and Würzburg-Dresden Cluster of Excellence ct.qmat, 01062 Dresden, Germany*
[4]*Department of Materials Science and Engineering, Stanford University, Stanford, CA 94035, USA*

(Dated: December 15, 2020)

We investigate charge pumping in the vicinity of order-obstructed topological phases, i.e. symmetry protected topological phases masked by spontaneous symmetry breaking in the presence of strong correlations. To explore this, we study a prototypical Su-Schrieffer-Heeger model with finite-range interaction that gives rise to orbital charge density wave order, and characterize the impact of this order on the model's topological properties. In the ordered phase, where the many-body topological invariant loses quantization, we find that not only is quantized charge pumping still possible, but it is even assisted by the collective nature of the orbital charge density wave order. Remarkably, we show that the Thouless pump scenario may be used to uncover the underlying topology of order-obstructed phases.

The robust quantization of transport properties observed in topological states of quantum matter is among the most fascinating phenomena in physics [1, 2], both from a fundamental perspective and due to its far-ranging potential for technological applications [3–5]. A primary example along these lines is provided by the integer quantum Hall effect [6, 7] in two-dimensional systems with a finite Chern number [8], as induced by a strong perpendicular magnetic field. Seminal work by Laughlin [9] and Thouless [10] has revealed that this topologically quantized charge transport may be understood as a cyclic adiabatic pumping process in time-dependent one-dimensional systems. While these intriguing phenomena can be understood within the independent particle approximation in the framework of topological Bloch bands [2], their stability against imperfections such as disorder and weak to moderate correlations is well established [1, 11, 12]. In strongly correlated systems however, qualitative changes to this picture occur, including the breakdown of topological band theory due to spontaneous symmetry breaking [13, 14] and dynamical quantum fluctuations [15–17], respectively, but also the formation of genuinely correlated topologically ordered phases [18].

In this work, we demonstrate how spontaneous symmetry breaking can facilitate and even drive quantized charge pumping (see sketch in Fig. 1). Remarkably, by means of unbiased numerical simulations, we show that this mechanism survives even in a strongly correlated regime, where an effective single-particle picture is found to break down, and would not correctly predict the adiabatic pumping properties. In particular, we observe that the Resta polarization [19] provides an unambiguous many-body topological characterization that agrees with direct calculation of the relevant transport properties. Furthermore, we reveal how the Thouless charge pumping approach [10, 20] can be used to characterize the buried topological phase diagram of order-obstructed phases, i.e. conventionally ordered phases that arise from symmetry protected topological (SPT) phases [21] by spontaneous symmetry breaking. We also note related recent works on the interplay between topology and symmetry breaking [22–24], as well as other work on fractional quantized charge pumping [25, 26], and on topology in strongly correlated systems [27].

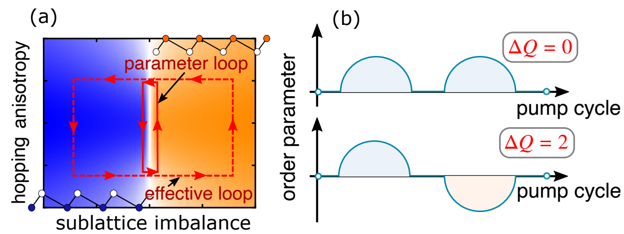

FIG. 1. Schematic of correlation-assisted charge pumping. (a): Sketch of correlation-assisted pump cycle in parameter space (solid line) and the effective parameter cycle in the absence of correlations (dashed line). Blue and red background in phase diagram denote orbital character of sublattice ordering (sublattice A and B respectively). (b): Sketch of order parameter over two correlation-assisted pump cycles which do not (upper) and do (lower) pump non-zero charge. Both cycles enter and exit the ordered phase, but only in the bottom cycle, corresponding to the cycle in (a), does the ordering change orbital character, leading to non-zero pumped charge.

To this end, we study in the framework of density matrix renormalization group (DMRG) methods [28, 29] a variant of the Su-Schrieffer-Heeger (SSH) model [30, 31] with finite-range interaction as a conceptually simple system exhibiting rich interplay between SPT phases and long-range order. For strong interactions, our model system exhibits an orbital charge-density wave (CDW) which spontaneously breaks the protecting chiral symmetry, exemplifying the aforementioned class of order-obstructed phases. Our findings closely connect to current experimental activity on realizing topological band structures with ultracold atoms in optical lattices [32–36], and may be verified in a strongly interacting version of recent experiments on quantized charge pumping in such settings [37, 38].

Model and Methods. — Initially conceived as a microscopic description of solitons in polyacetylene [31], the SSH model has become a prototype for topological physics in one-dimensional systems. Several interacting variants of the SSH model have been studied in previous literature [39–41], where extended interactions have been seen to give rise to exotic collective phases of matter [42]. Here, considering a extended interaction $\hat{V}$ that retains both chiral and particle hole symmetry [43, 44], we demonstrate how the interplay of SPT order and spontaneous symmetry breaking conspire to exhibit interesting, previously undocumented behavior.

The particular model we study is described by the microscopic Hamiltonian:

$$\hat{H} = -\sum_j \left(J\hat{b}_j^\dagger \hat{a}_j + \frac{d+\tau}{2}\hat{b}_j^\dagger \hat{a}_{j+1} + \frac{d-\tau}{2}\hat{a}_j^\dagger \hat{b}_{j+1} \right) + \text{h.c.}$$
$$+ \quad V\sum_j \left(\hat{n}_j^a \hat{n}_{j+1}^b + \hat{n}_j^b \hat{n}_{j+1}^a \right), \tag{1}$$

on a bipartite chain of spinless fermions with two orbitals per site (a and b). $\hat{a}_j^\dagger(\hat{a}_j)$ and $\hat{b}_j^\dagger(\hat{b}_j)$ represent creation (annihilation) operators on orbitals in sublattice a and b respectively, on site j. J is an intra-cell hopping [45], and $(d \pm \tau)/2$ are alternating inter-cell inter-orbital hopping strengths. In the second summation, $\hat{V}$, $\hat{n}^a = \hat{a}^\dagger \hat{a}$, and likewise for $\hat{n}^b$. To investigate this model, we use the DMRG technique [29]. Below, we show results for periodic boundary conditions (PBC). In the Supplementary Material [46] (see also references [47–49] therein), we present analogous results for systems with open boundary conditions (OBC) and extensively compare the two. For DMRG and system details, see [46].

To probe topological properties of our model (1), we focus on two many-body topological invariants. First, the Resta (many-body) polarization for periodic systems [19],

$$P = \frac{qa_0}{2\pi}\text{Im}\ln\text{Tr}\left[\hat{\rho}\, e^{\frac{i2\pi}{La_0}\hat{X}}\right] \quad (\text{mod}\, qa_0)\,, \tag{2}$$

where a_0 is the lattice spacing, L is the number of unit cells, and $\hat{X} = \sum_i x_i \hat{n}_i$ is the many-body center of mass operator; $\hat{\rho}$ denotes the many-body density matrix [50]. Second, we study the entanglement spectrum [51–53], which is intimately connected to the Resta polarization [54], and to charge pumping [55]. It has also been studied specifically in the context of the SSH model [56]. To define this, we consider the reduced density matrix resulting from tracing out half of our system across a spatial bipartition: $\rho_L = \text{Tr}_R[\rho_{LR}]$. The entanglement spectrum is the set of ordered eigenvalues λ_i of the entanglement Hamiltonian $\mathcal{H}_E = -\log\rho_L$. The degeneracies of the spectrum are determined by fundamental characteristics of the state, including topological properties and symmetries such as inversion symmetry. We define the *entanglement gap* as $\Delta\lambda = \lambda_1 - \lambda_0$.

Phase Diagram. — For concreteness, we focus on the phase diagram slice for $d = 0.4, \tau = 1.0$ (cf. Fig. 2 (a)). However, we investigated many parameter combinations and found that the qualitative behavior is generally preserved across the parameter regimes considered. Roughly, increasing d shifts the trivial-topological phase boundary to the right, and τ does not have much impact on the topological properties (as long as $\tau \neq 0$). Our designations of trivial and topological regions in the phase diagram are determined by the value of the polarization (2) in the normal phase (defined by explicitly suppressing CDW order). This is consistent with our complementary classification approach by entanglement. CDW order can be identified by the change in ground state degeneracy [57].

In the resulting phase diagram of the SSH model with interaction (1), we identify four different phases, distinguished by the presence or absence of SPT order and CDW order (see Fig. 2 (a)). The first two phases, band insulator (BI) and topological insulator (TI) are present without interaction and persist for weak to moderate interaction. For sufficiently strong interaction (indicated by the black squares in Fig. 2 (a)), spontaneous orbital CDW order emerges (see [46]), which obstructs the underlying topology. The two resulting phases, OOBI and OOTI, are characterized by sublattice symmetry breaking. Their topological properties are discussed below. We checked that the phase diagram is not qualitatively changed by the addition of other small terms obeying chiral symmetry, or by the presence of a small intra-cell interaction $\hat{U}$. Subsequently, we elaborate on all four phases, going through the phase diagram in Fig. 2 (a) from weak to strong interactions.

For $V = 0$, the Hamiltonian can be expressed in the single-particle basis, and all topological information can also be extracted from the single particle density matrix (SPDM) by decomposing $\rho_k(t) = \frac{1}{2}\left[1 - \mathbf{r}_k(t)\cdot\sigma\right]$ in momentum-space, where

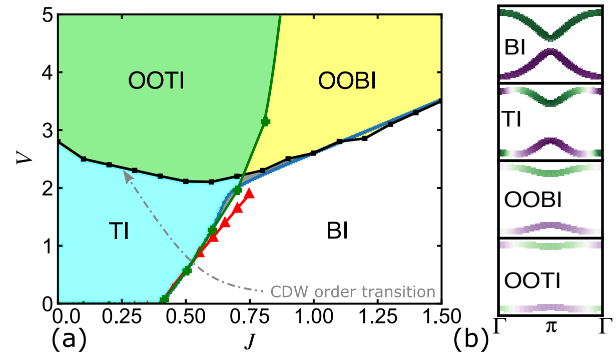

FIG. 2. (a): Phase diagram for interacting SSH model with $d = 0.4$, $\tau = 1.0$. **TI**: Topological Insulator, **BI**: Band Insulator, **OOBI**: Order-obstructed Band Insulator, **OOTI**: Order-obstructed Topological Insulator. Red triangles denote mean field theory (MFT) results for **BI** → **TI** phase boundary. Black squares denote finite size scaling calculations from fitting the orbital CDW phase transition to Ising universality class. The blue line delineates regions of single (right) and double (left) ground state degeneracy for OBC systems. Green '+' and solid green line indicates polarization phase boundary. Simulations were performed on systems with up to $L = 100$ unit cells. Gray shading in center represents region of uncertainty given the accessible system sizes. (b): Typical band structures in each phase. Color signifies orbital character with respect to the BI basis, and level of transparency represents strength of band mixing.

$\mathbf{r}_k$ is the pseudospin vector. In equilibrium, the quantity ν, defined by $(-1)^\nu = \mathrm{sgn}(r^x_\Gamma r^x_\pi)$, coincides with the pseudospin winding number [58]: $\mathcal{W} = \frac{1}{2\pi}\int_{-\pi/a}^{\pi/a} dk(n^x_k\partial_k n^y_k - n^y_k\partial_k n^x_k)$, where $\mathbf{n}_k = \mathbf{r}_k/|\mathbf{r}_k|$. A nontrivial value of either invariant is equivalent to the condition $|d| > |J|$, and a topological phase transition occurs when $|\mathbf{r}_\Gamma| = 0$, at which point r^x_Γ changes sign. One can also view the SPDM as the density matrix corresponding to the (in the presence of interactions, mixed) state of some auxiliary Hamiltonian, $\rho_k = e^{-\mathcal{H}_k}$ [59], and can use $\mathcal{H}_k$ to compute the Zak phase [60] from its eigenstates: $\mathcal{Z} = \frac{i}{\pi}\int_{-\pi/a}^{\pi/a} dk\langle\phi_k|\partial_k\phi_k\rangle$. The Zak phase is quantized to $\mathcal{Z} = \nu$ and can be used as a topological invariant in the non-interacting SSH model; it is also equivalent to the quantized polarization, $P = \nu q a_0/2$.

When weak interaction (preserving chiral symmetry) is added to the model, the Zak phase and the topological invariant extracted from the SPDM both agree with the Resta polarization. This reflects the fact that the SPDM still contains most of the information about the many-body topology [46]. The positive slope of the BI → TI phase boundary can be attributed to (even at mean-field level) the interaction pushing valence and conduction bands closer together, facilitating hybridization. As illustrated in the band-structure sketches in Fig. 2 (b), the TI phase is characterized by band inversion at the Γ-point.

Strong interaction favors the emergence of orbital CDW order with ground states that spontaneously break chiral symmetry. When explicitly suppressing CDW order (thus enforcing chiral symmetry), the solid green line in Fig. 2 (a) still separates the topological insulator from the trivial insulator phase. In this scenario, we can distinguish these two phases by their polarization ($P = 0$ for trivial, $P = \pm q a_0/2$ for topological) even within the unstable region where in principle charge order would obstruct the SPT phases. Furthermore, the strongly interacting topological region still features edge modes. When allowing for CDW order, the topologically trivial phase defines the OOBI region in Fig. 2 (a) within which no charge can be pumped, and the topological phase defines the OOTI region in Fig. 2 (a), within which quantized charge pumping is possible as shown below.

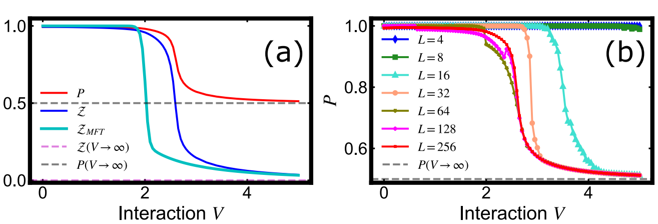

FIG. 3. Fractionalization in the symmetry broken phase, with $J = 0.1$, $d = 0.4$, $\tau = 1.0$. (a) Resta polarization P computed using DMRG, and the Zak phase, computed from DMRG and MFT for $L = 256$ unit cells. In infinite V limit in the symmetry broken phase, $\mathcal{Z} \to 0$ and $P \to \pm q a_0/4$. (b) System-size dependence of the polarization. Polarization curve converges with system-size, but does not obey finite-size scaling. P is in units of $q a_0/2$.

Nevertheless, even in the order obstructed regime, important signatures of the inherited topological properties persist, as illustrated in Fig. 2 (b). The trivial OOBI has a band structure similar to BI, but with strong band mixing close to the Γ-point. The band structure of OOTI combines features of TI and OOBI: band inversion and band mixing. The onset of orbital order for transitions TI → OOTI and BI → OOBI can be identified by entanglement signatures in the symmetry broken state [46]. In the band insulating phase, the transition is accompanied by an abrupt change in the slope of the entanglement entropy. In the TI phase, the entanglement gap is $\Delta\lambda = 0$, and becomes non-zero upon emergence of orbital order. In the OOTI phase, the edge states are gapped out. Remarkably, even in the presence of CDW order, we will demonstrate that adiabatic charge pumping still allows us to distinguish the OOTI from the OOBI region, as separated by the solid green line in Fig. 2 (a).

To compare the single-particle and the many-body characterization of the topology, we compute the natural orbitals $|\phi_k\rangle$ from the SPDM as the best choice of a single-particle basis and the corresponding Zak phase $\mathcal{Z}$. The breakdown of such single-particle topological invariants was previously documented [61]. Remarkably, the Resta polarization P and $\mathcal{Z}$ agree well for large parts of the phase diagram. In the normal phase, both $\mathcal{Z}$ and P remain quantized, and the two quantities align for all V [62]. In the ordered phase, both P and $\mathcal{Z}$ fractionalize (Fig. 3 (a)). In the large V limit, hallmarking the breakdown of the single-particle picture, the polarization of the degenerate ground states approaches the fractionalized values $P = \pm q a_0/4$ [63], and the Zak phase converges towards $\mathcal{Z} = 0$. Fig. 3 (b) illustrates the system-size dependence of the P. While P (as a function of V) converges with system-size, it inherits only indirectly from the CDW order, and as such does not obey the same scaling collapse.

Charge Pumping. — Despite the fact that polarization (2) is not quantized in the ordered phase, we find that the underlying topological character of the phase without broken symmetry is present in the adiabatic transport properties of the system. One can imagine adding a (infintesimally small) staggered on-site potential term $\hat{\Delta} = \Delta\sum_j(\hat{n}^a_j - \hat{n}^b_j)$ to the model, which acts as a pinning field. The point $\Delta = \tau = 0$ is the degeneracy point, at which the system has no preference for either sub-orbitals a or b. Adiabatically looping around this degeneracy point through cyclic variation of Δ and τ, quantized charge

$$\Delta Q = \frac{1}{a}\int_0^T dt\,\partial_t P(t), \tag{3}$$

is transported. In practice, we compute $P(t)$ along the cycle from the instantaneous Hamiltonian $\hat{H}(\theta)$ with the loop variable $\theta \in [0, 2\pi]$ [64].

Inspecting ΔQ across the phase diagram Fig. 2 (a), we find that the topological character of the underlying state *without* broken symmetry is recovered. While this behavior is expected for the weakly-interacting TI phase, it is remarkable that the obstructed OOTI phase (with $P \neq 0$ without broken

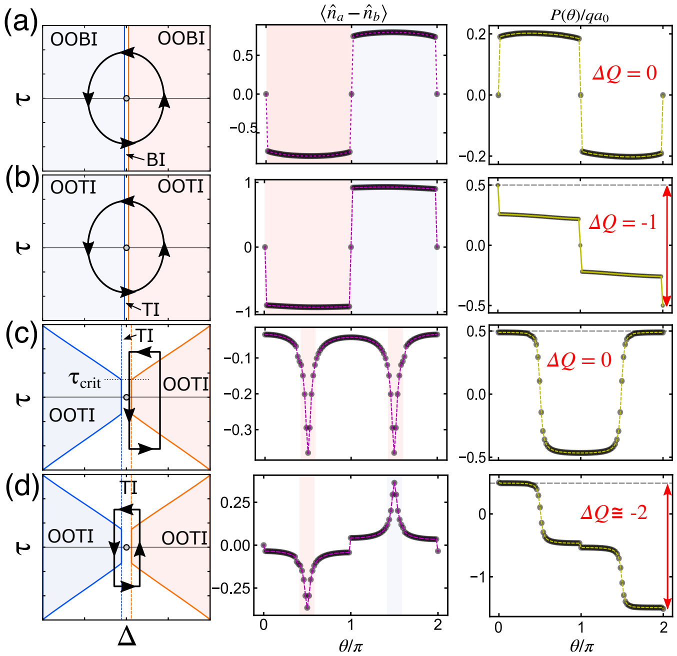

FIG. 4. Correlation-assisted Thouless pump cycles. Left panel: sketch of cycle in phase diagram. Center panel: order parameter along cycle. Right panel: polarization along cycle. (a) and (b): Pump cycles within (a) OOBI and (b) OOTI phases. In (c) and (d), the system enters and exits the ordered phase. (d) successfully transports charge, but (c) does not. Shaded blue (orange) regions denote orbital ordering with occupation localized on sublattice a (b), across which the order parameter attains peak magnitude in the thermodynamic limit. In numerics, (d) transports charge $\Delta Q = -2.010(4)$, which is asymptotically quantized to $\Delta Q \to 2$ in the thermodynamic limit. Each cycle performed by adiabatically connecting 100 independent ground state calculations, for systems of $L = 100$ unit cells. Specific parameter values used to generate these results are detailed in Table I in the Supplementary material [46].

symmetry) is characterized by quantized $\Delta Q \neq 0$. This is demonstrated in Fig. 4 (a)–(d).

The unit of quantization in OOTI is $1/2$ that of the TI phase, reflecting the fractionalization of excitations in the presence of orbital order. Additionally, while charge is pumped continuously in TI, in OOTI charge is mostly pumped in discrete jumps, *driven* by the collective order.

These jumps are easily understood in the context of sublattice filling: The cycle begins with the system in the insulating phase. Very abruptly the onset of order leads to orbital occupation supported primarily on sublattice a. This 'jump' is accomplished by shifting half of the electron occupation (the occupation of sublattice b orbitals) to the a orbital on the same site. When $\theta = \pi$, Δ changes sign, quickly altering the energy landscape to favor occupation on b rather than a. In this moment, the second jump occurs as all of the electrons shift to the neighboring sublattice b. Finally, the system re-enters the topological insulating phase and half of the occupation moves from b to the a orbital on the same site. Altogether, one unit of charge is pumped during this cycle. Also note that the jump at $\theta = \pi$ is twice as large as the other jumps, as *all* rather than half of the occupation shifts one orbital.

Moreover, the single-particle picture of charge pumping breaks down in the presence of strong interactions. An effective single-particle description is obtained from integrating the Berry curvature of the natural orbitals $\Omega(k,t) = 2\,\mathrm{Im}\langle \partial_k \phi_k(t) | \partial_t \phi_k(t) \rangle$: $\Delta Q = (q/2\pi) \int dk \int dt \Omega(k,t) n(k,t)$, where $n(k,t)$ is the larger occupation eigenvalue. Similar to Ref. [55], we find that the non-uniform $n(k,t)$ along the cycle leads to non-quantized ΔQ in this single-particle picture.

Whereas the pump cycles in Fig. 4 (a) and (b) demonstrate that charge pumping remains quantized in the order-obstructed phase, Fig. 4 (c) and (d) illustrate how charge pumping is facilitated by the collective nature of the obstructing order. For these two cycles, there is a critical τ that controls whether or not there is orbital ordering when an infinitesimal seed is added. As such, these cycles utilize the spontaneous symmetry breaking of the ground state to minimize reliance on on-site staggered potential Δ. In the ordered phase, orbital character of the state is completely determined by the sign of Δ, independent of magnitude. Thus, one can exert control over the orbital character (for τ in the right region) via infinitesimal staggered onsite potential (or any other mechanism which acts as a seed for the order). In (c), both times τ becomes small enough to induce ordering it settles on the same orbital character, resulting in net zero charge pumped. In (d) however, Δ changes sign, leading to four jumps in sublattice occupation (or two pairs of jumps).

As $|\tau| \to 0$, the system spontaneously orders before reaching the degeneracy point, avoiding the band-gap closing [65]. Since this spontaneous ordering randomly picks a direction, not all pump cycles will transport net charge, as demonstrated in Fig. 4 (c). If the sign of the order coincides with that of τ as in Fig. 4 (d), then charge is indeed transported. This illustrates the possibility of quantized charge transport with neither bias nor staggered potential.

In this example, the correlation-assistance to charge pumping comes in the form of eliminating the staggered potential, enabling quantized pumping by only varying the hopping anisotropy. In general, it operationally means one can nontrivially control charge pumping via a single tunable parameter, greatly increasing feasibility of experimental efforts [66].

Concluding discussion. — In summary, we have described and characterized the effect of spontaneous symmetry breaking on many-body topology, and have shown that the Thouless pump can be used to identify underlying topology in order-obstructed phases. Moreover, we illustrate that collective order can be conducive to quantized charge transport, with spontaneous ordering working to prevent band gap closing even when the model is tuned to the degeneracy point. En route to demonstrating this effect, we have presented a complete phase diagram for an SSH model with extended interaction, including a phase in which orbital charge density wave order obstructs topology. Our model may be realized in state of the art experiments on cold-atoms in optical lattices [37].

The correlation-assisted charge pumping we demonstrate in the interacting SSH model should be typical of the interplay between topology and collective order. In our present case of a spontaneously broken $\mathbb{Z}_2$ symmetry, random fluctuations alone suffice to produce quantized charge transport. For other symmetries, what survives is that only an infinitesimally small external potential is needed to control transport processes. The collective phase can be exploited to circumvent the many-body topological constraint in real-time evolution, where the topological invariant is pinned to its initial value under unitary evolution. Hence, a dynamical topological phase transition can be induced by passing through the symmetry breaking collective phase, giving rise to dynamically induced symmetry breaking [67]. This principle can be generalized to ordered phases obstructing other SPT states.

Acknowledgements. – DMRG calculations were performed using the ITensor library [68]. We thank Miles E. Stoudenmire for helpful discussions regarding time evolution of Fermionic systems in ITensor. We also thank the Stanford Research Computing Center for providing computational resources. Data used in this manuscript is stored on Stanford's Sherlock computing cluster. Supported by the U.S. Department of Energy (DOE), Office of Basic Energy Sciences, Division of Materials Sciences and Engineering, under contract DE-AC02-76SF00515. M. S. thanks the Alexander von Humboldt Foundation for its support with a Feodor Lynen scholarship. J.C.B. acknowledges financial support from the German Research Foundation (DFG) through the Collaborative Research Centre SFB 1143 (Project No. 247310070) and the Würzburg-Dresden Cluster of Excellence on Complexity and Topology in Quantum Matter – ct.qmat (EXC 2147, Project No. 39085490).

* jamarks@stanford.edu
† schuelem@stanford.edu

[1] M. Z. Hasan and C. L. Kane, Rev. Mod. Phys. **82**, 3045 (2010).
[2] X.-L. Qi and S.-C. Zhang, Rev. Mod. Phys. **83**, 1057 (2011).
[3] C.-Z. Chang, J. Zhang, X. Feng, J. Shen, Z. Zhang, M. Guo, K. Li, Y. Ou, P. Wei, L.-L. Wang, Z.-Q. Ji, Y. Feng, S. Ji, X. Chen, J. Jia, X. Dai, Z. Fang, S.-C. Zhang, K. He, Y. Wang, L. Lu, X.-C. Ma, and Q.-K. Xue, Science **340**, 167 (2013).
[4] M. König, S. Wiedmann, C. Brüne, A. Roth, H. Buhmann, L. W. Molenkamp, X.-L. Qi, and S.-C. Zhang, Science **318**, 766 (2007).
[5] Z. Yue, G. Xue, J. Liu, Y. Wang, and M. Gu, Nat Commun **8**, 1 (2017).
[6] K. v. Klitzing, G. Dorda, and M. Pepper, Phys. Rev. Lett. **45**, 494 (1980).
[7] R. Prange and S. Girvin, *The Quantum Hall effect*, Graduate texts in contemporary physics (Springer-Verlag, 1987).
[8] D. J. Thouless, M. Kohmoto, M. P. Nightingale, and M. den Nijs, Phys. Rev. Lett. **49**, 405 (1982).
[9] R. B. Laughlin, Phys. Rev. B **23**, 5632 (1981).
[10] D. J. Thouless, Phys. Rev. B **27**, 6083 (1983).
[11] F. D. M. Haldane, Phys. Rev. Lett. **61**, 2015 (1988).
[12] X.-L. Qi, T. L. Hughes, and S.-C. Zhang, Phys. Rev. B **78**, 195424 (2008).
[13] S. Rachel, D. Schuricht, B. Scharfenberger, R. Thomale, and M. Greiter, Journal of Physics: Conference Series **200**, 022049 (2010).
[14] M. Hohenadler, T. C. Lang, and F. F. Assaad, Phys. Rev. Lett. **106**, 100403 (2011).
[15] J. C. Budich, R. Thomale, G. Li, M. Laubach, and S.-C. Zhang, Phys. Rev. B **86**, 201407(R) (2012).
[16] W. Witczak-Krempa, M. Knap, and D. Abanin, Phys. Rev. Lett. **113**, 136402 (2014).
[17] A. Amaricci, J. C. Budich, M. Capone, B. Trauzettel, and G. Sangiovanni, Phys. Rev. Lett. **114**, 185701 (2015).
[18] X.-G. Wen, Rev. Mod. Phys. **89**, 041004 (2017).
[19] R. Resta, Phys. Rev. Lett. **80**, 1800 (1998).
[20] Q. Niu and D. J. Thouless, J. Phys. A: Math. Gen. **17**, 2453 (1984).
[21] X. Chen, Z.-C. Gu, Z.-X. Liu, and X.-G. Wen, Phys. Rev. B **87**, 155114 (2013).
[22] D. González-Cuadra, A. Dauphin, P. R. Grzybowski, P. Wójcik, M. Lewenstein, and A. Bermudez, Phys. Rev. B **99**, 045139 (2019).
[23] D. González-Cuadra, A. Bermudez, P. R. Grzybowski, M. Lewenstein, and A. Dauphin, Nature Communications **10**, 10.1038/s41467-019-10796-8 (2019).
[24] D. González-Cuadra, A. Dauphin, P. R. Grzybowski, M. Lewenstein, and A. Bermudez, $\mathbb{Z}_n$ solitons in intertwined topological phases (2019), arXiv:1908.02186 [cond-mat.quant-gas].
[25] P. Marra, R. Citro, and C. Ortix, Phys. Rev. B **91**, 125411 (2015).
[26] R. Li and M. Fleischhauer, Phys. Rev. B **96**, 085444 (2017).
[27] B. Hetényi, Physical Review Research **2**, 10.1103/physrevresearch.2.023277 (2020).
[28] S. R. White, Phys. Rev. Lett. **69**, 2863 (1992).
[29] U. Schollwöck, Rev. Mod. Phys. **77**, 259 (2005).
[30] W. P. Su, J. R. Schrieffer, and A. J. Heeger, Phys. Rev. Lett. **42**, 1698 (1979).
[31] A. J. Heeger, S. Kivelson, J. R. Schrieffer, and W. P. Su, Rev. Mod. Phys. **60**, 781 (1988).
[32] M. Aidelsburger, M. Atala, S. Nascimbène, S. Trotzky, Y.-A. Chen, and I. Bloch, Phys. Rev. Lett. **107**, 255301 (2011).
[33] J. Struck, C. Ölschläger, M. Weinberg, P. Hauke, J. Simonet, A. Eckardt, M. Lewenstein, K. Sengstock, and P. Windpassinger, Phys. Rev. Lett. **108**, 225304 (2012).
[34] N. Goldman, J. C. Budich, and P. Zoller, Nature Phys. **12**, 639 (2016).
[35] A. Dauphin, D.-T. Tran, M. Lewenstein, and N. Goldman, 2D Mater. **4**, 024010 (2017).
[36] N. Fläschner, B. S. Rem, M. Tarnowski, D. Vogel, D.-S. Lühmann, K. Sengstock, and C. Weitenberg, Science **352**, 1091 (2016).
[37] M. Lohse, C. Schweizer, O. Zilberberg, M. Aidelsburger, and I. Bloch, Nature Phys. **12**, 350 (2016).
[38] S. Nakajima, T. Tomita, S. Taie, T. Ichinose, H. Ozawa, L. Wang, M. Troyer, and Y. Takahashi, Nature Phys. **12**, 296 (2016).
[39] J. Jünemann, A. Piga, S.-J. Ran, M. Lewenstein, M. Rizzi, and A. Bermudez, Phys. Rev. X **7**, 031057 (2017).
[40] B. Sbierski and C. Karrasch, Phys. Rev. B **98**, 165101 (2018).
[41] A. M. Marques and R. G. Dias, Phys. Rev. B **95**, 115443 (2017).
[42] E. Anisimovas, M. Račiūnas, C. Sträter, A. Eckardt, I. B. Spielman, and G. Juzeliūnas, Phys. Rev. A **94**, 063632 (2016).
[43] A. Kruckenhauser and J. C. Budich, Phys. Rev. B **98**, 195124 (2018).
[44] Unlike the intracell interaction $\hat{U} = U\sum_j \hat{n}_j^a \hat{n}_j^b$, $\hat{V}$ is efficient at thermalizing, which is important for dynamically preparing such phases.

[45] Our analysis strictly excludes the point $J = 0$, at which the model obeys different symmetries.

[46] Supplemental material, available online.

[47] C.-E. Bardyn, L. Wawer, A. Altland, M. Fleischhauer, and S. Diehl, Phys. Rev. X **8**, 011035 (2018).

[48] L. Fu and C. L. Kane, Phys. Rev. B **74**, 195312 (2006).

[49] A. Altland and M. R. Zirnbauer, Phys. Rev. B **55**, 1142 (1997).

[50] P defined in this way is only strictly valid as a topological invariant for periodic systems. The polarization for OBC systems is defined as $P_{OBC} = q\langle \hat{X} \rangle$. However, P is still well-defined for OBC systems as long as the effects of single particle edge modes are restricted to the boundaries.

[51] F. Pollmann, A. M. Turner, E. Berg, and M. Oshikawa, Phys. Rev. B **81**, 064439 (2010).

[52] L. Fidkowski and A. Kitaev, Phys. Rev. B **83**, 075103 (2011).

[53] H. Li and F. D. M. Haldane, Phys. Rev. Lett. **101**, 010504 (2008).

[54] M. P. Zaletel, R. S. K. Mong, and F. Pollmann, Journal of Statistical Mechanics: Theory and Experiment **2014**, P10007 (2014).

[55] A. Hayward, C. Schweizer, M. Lohse, M. Aidelsburger, and F. Heidrich-Meisner, Phys. Rev. B **98**, 245148 (2018).

[56] S. Ryu and Y. Hatsugai, Phys. Rev. B **73**, 245115 (2006).

[57] This is true for PBC systems, where only the OOTI and OOBI phases have doubly degenerate ground states. For OBC systems the TI phase does as well, as illustrated by the blue line in 2 (a). More sophisticated measures must be taken for OBC systems, as detailed in the Supplementary Material [46].

[58] B. Pérez-González, M. Bello, A. Gómez-León, and G. Platero, arXiv:1802.03973 [cond-mat] (2018).

[59] In equilibrium, $\mathcal{H}_k$ is proportional to the single-particle Hamiltonian.

[60] J. Zak, Phys. Rev. Lett. **62**, 2747 (1989).

[61] F. Grusdt, N. Y. Yao, and E. A. Demler, Phys. Rev. B **100**, 075126 (2019).

[62] For OBC systems, P is well-behaved in the symmetry broken phase (in qualitative agreement with PBC), in the normal phase experiences a boundary-driven transition for moderate system sizes. This (finite-size effect) transition, which is due to edge states hybridizing with the bulk, disappears in the thermodynamic limit.

[63] The fractionalized value for P is intrinsically due to CDW order.

[64] We have also performed these cycles explicitly via time evolution on small systems. The results are presented in the Supplementary Material [46].

[65] Due to finite-size effects, we were forced to used small pinning field $|\Delta| = 10^{-2}$ throughout. In the thermodynamic limit however, $\Delta = 0$ would also work (the collective order can be induced by random fluctuations).

[66] These correlations also allow us to realize faster pumps, as explicitly illustrated in [46].

[67] M. McGinley and N. R. Cooper, Phys. Rev. Lett. **121**, 090401 (2018).

[68] ITensor Library.